ECMOR XVI
16TH EUROPEAN CONFERENCE ON THE MATHEMATICS OF OIL RECOVERY

EAGE

P032

Algebraic Dynamic Multilevel Method for Single-phase Flow in Heterogeneous Geothermal Reservoirs

M. HosseiniMehr* (TU Delft), R.B. Arbarim (TU Delft), M. Cusini (TU Delft), C. Vuik (TU Delft), H. Hajibeygi (TU Delft)

Summary

Accurate numerical simulation of coupled fluid flow and heat transfer in heterogeneous geothermal reservoirs demand for high resolution computational grids. The resulting fine-scale discrete systems--though crucial for accurate predictions--are typically upscaled to lower resolution systems due to computational efficiency concerns. Therefore, advanced scalable methods which are efficient and accurate for real-field applications are more than ever on demand. To address this need, we present an algebraic dynamic multilevel method for flow and heat transfer in heterogeneous formations, which allows for different temperature values for fluid and rock. The fine-scale fully-implicit discrete system is mapped to a dynamic multilevel grid, the solution at which are connected through local basis functions. These dynamic grid cells are imposed such that the sub-domain of sharp gradients are resolved at fine-scale, while the rest of the domain remains at lower (coarser) resolutions. In order to guarantee the quality of the local (heat front) components, advanced multiscale basis functions are employed for global (fluid pressure and rock temperature) unknowns at coarser grids. Numerical test cases are presented for homogeneous and heterogeneous domains, where ADM employs only a small fraction of the fine-scale grids to find accurate complex nonlinear thermal flow solutions. As such, it develops a promising scalable framework for field-scale geothermal simulations.

Introduction

Geothermal energy is an attractive resource to reduce the carbon footprint in the environment while providing affordable energy to society, and is expected to increase its contribution for years to come (Bertani, 2012; Lund et al., 2011; Burnell et al., 2012, 2015). The successful implementation of the field-scale projects, now more than ever, depends on accurate highly-resolved models that describe the flow and transport of mass and heat in heterogeneous (possibly fractured and faulted) reservoirs (OSullivan et al., 2001; Axelsson et al., 2003). In addition, when operated close to the faults, the geomechanical impact of the fluid-driven heat transfer becomes a key aspect in maintaining the safety standards (David and Jenny, 2016; Norbeck et al., 2018; Norbeck and Horne, 2016; Deb and Jenny, 2017).

The field-relevant simulation approaches face a number of challenges, among which some stand out. One of the main challenges is due to the highly heterogeneous fine-scale rock hydraulic and conductive properties, which demands for high resolution grids over the entire domain of study. At the same time, as another important challenge, the coupling of heat and mass transfer can impose sever stability issues for which proper formulation (choice of unknowns) and careful coupling treatments are crucial (Wong et al., 2018; Praditia et al., 2018). Fluid physics, production geochemistry (Morel and Morgan, 1972; Leal et al., 2017), and geomechanical effects (Rossi et al., 2018) are also among the challenges that collectively contribute to the complexity of development of next-generation geothermal simulators, with both their demand for high-resolution grids and nonlinear coupling. As such, of particular interest is to develop a stable simulation method which is scalable to the field-relevant applications and avoid excessive use of upscaled coefficients.

This paper describes a scalable framework for field-scale simulation of the geothermal reservoirs. The fine-scale reference system is obtained by using the fully-implicit flow-heat (i.e., Pressure-Temperature (P-T)) integration scheme, where the fluid (and possibly rock) properties are obtained after each P-T Newton updates. The fully-implicit nature of the discrete formulation would ensure its stability in presence of strong non-linear terms. The fine-scale system considers both conductive and convective heat transfer terms, and allows for different temperature values for the fluid and reservoir rock. Such a consideration would increase the simulation accuracy, specially for heterogeneous (and fractured) systems, where the fluid and rock heat transfer regimes can be in very different time scales.

The given fully-implicit system at fine-scale is then mapped to an algebraically-developed dynamic multilevel resolution. The dynamic multilevel resolution is obtained based on a front tracking technique, where the sub-domain of sharp gradients are being resolved at the fine scale, and the rest of the domain in a hierarchical nested coarser resolutions. Similar to the ADM framework (Cusini et al., 2016), the map between the solution (unknowns) at different resolutions is constructed by local basis functions, which are computed only at the beginning of the time-dependent simulation. Note that these basis functions will never get updated through out the entire simulation. Here, we develop local basis functions to interpolate the solution for pressure (P), rock (T_r) and fluid (T_f) temperatures. For the pressure and rock temperatures, multiscale basis functions (Hou and Wu, 1997; Jenny et al., 2003; Hajibeygi et al., 2008; Wang et al., 2014) are developed for the ADM multilevel system. Due to its similarities with the phase saturation equation, the fluid temperature from coarser to finer scales are obtained using constant interpolation functions. The dynamic grid is expected to capture the heat front; in another words, when coarser grids are employed, the temperature gradients are smaller than the prescribed threshold. Note that the scope of this paper is about structured grids, and that unstructured multiscale basis functions (Møyner and Lie, 2016; Bosma et al., 2017; Parramore et al., 2016) are required for unstructured ADM.

The proposed ADM method constructs an accurate fully-implicit (thus stable) multi-level dynamic system, which reduces the computational complexity and at the same time maintains the simulation accuracy to the desired tolerance levels. Note that the ADM solutions for pressure and temperature can be interpolated to the finest scale, if needed, e.g., for phase property update. Numerical test cases for both homogeneous and heterogeneous test cases are presented, as proof-of-the-concept, to illustrate the accuracy and applicability of the devised method. It is shown that only a small fraction of the fine-scale grid cells are sufficient, if the developed multiscale-based prolongation and restriction operators are being

used, to find a good approximate solution to the fine-scale expensive simulations.

The paper is organised as follows. The governing equations and the fine-scale discretisation are presented in the following section. The ADM method for geothermal simulations is described in Section 3. Numerical results and concluding remarks are presented in Sections 4 and 5, respectively.

Governing equations & fine-scale discretization

Mass balance equation for non-isothermal single-phase flow in a heterogeneous porous medium is described by

$$\frac{\partial}{\partial t}\left(\phi\rho_f\right) - \nabla\cdot\left(\rho_f\frac{1}{\mu_f}\mathbf{K}\cdot\nabla p\right) = \rho_f q, \tag{1}$$

where ϕ is the porosity of the rock, ρ_f and μ_f are fluid density and fluid viscosity, respectively. Additionally, $\mathbf{K}$ is the rock permeability tensor and q is the source term. In addition, the energy balance equation reads

$$\frac{\partial}{\partial t}\left(\phi\rho_f U_f\right) - \nabla\cdot\left(\rho_f H_f\frac{1}{\mu_f}\mathbf{K}\cdot\nabla p\right) = Ah(T_r - T_f) + \rho_f H_f q, \tag{2}$$

for the fluid, and

$$\frac{\partial}{\partial t}\left((1-\phi)\rho_r U_r\right) - \nabla\cdot\left(\mathbf{D}\cdot\nabla T_r\right) = Ah(T_f - T_r), \tag{3}$$

for the solid rock. Here, T is the temperature, U is the specific internal energy and H is the specific enthalpy. In general, U and H can be expressed as non-linear functions of temperature and pressure. The subscripts f and r indicate the fluid and the solid rock, respectively. Finally, $\mathbf{D}$ is the rock thermal conductivity tensor, A is the area of heat exchange between the rock and the fluid and h is the conduction-convection heat exchange coefficient (see Appendix). Remark that for most applications the area A is so large that the fluid and the rock can be considered in thermal equilibrium (i.e., $T = T_f = T_r$). In such a case, only two equations for the two unknowns P and T need to be solved. However, due to the heterogeneous hydraulic and conductive properties, e.g., in presence of fractures or in regions with very high convective terms (e.g., close to wells), such a hypothesis may not be valid.

Equations (1), (2) and (3), along with a set of constitutive laws, form a well-posed system of equations for the three main unknowns, i.e., p, T_f and T_r. The equations are discretised with a finite-volume scheme in space on a Cartesian grid and with an Euler backward method in time. Convective fluxes are discretised employing a two-point flux approximation (TPFA). Since the equations are non-linear, a Newton-Raphson iteration is employed to solve the system of equations iteratively. Thus, at each non-linear iteration ν, a linearised system of the form $\mathbf{J}_\mathbf{0}^\nu \delta\mathbf{x}_\mathbf{0}^{\nu+1} = -\mathbf{r}_\mathbf{0}^\nu$ has to be solved, i.e.,

$$\underbrace{\begin{bmatrix} J_{m_p} & J_{m_{T_f}} & J_{m_{T_r}} \\ J_{f_p} & J_{f_{T_f}} & J_{f_{T_r}} \\ J_{r_p} & J_{r_{T_f}} & J_{r_{T_r}} \end{bmatrix}}_{\mathbf{J}_0^\nu} \underbrace{\begin{bmatrix} \delta p \\ \delta T_f \\ \delta T_r \end{bmatrix}}_{\delta x_0^{\nu+1}} = -\underbrace{\begin{bmatrix} r_m \\ r_f \\ r_r \end{bmatrix}}_{r_0^\nu}. \tag{4}$$

Here, $\mathbf{J}_0^\nu$, $\delta x_0^{\nu+1}$ and r_0^ν are the Jacobian (derivatives) matrix, the vector of updates and the residual vector, respectively. Also, each block J_{e_α} contains the derivatives of equation e with respect to the unknown α, i.e. $J_{e_\alpha} = \partial r_e/\partial\alpha$. Subscripts m, f and r refer to equations of mass balance, energy balance in fluid and energy balance in the rock, respectively. Note that $J_{m_{T_r}} = 0$ holds, i.e., the fluid properties depend only on the fluid temperature T_f. The solution of the linear-system (4) is the most computationally expensive step for field-scale simulations on high-resolution grids. As such, field-scale relevant simulation approaches aim to develop a sclaable solution strategy for this coupled nonlinear system.

In this work, we develop the Algebraic Dynamic Multilevel method for fully-coupled geothermal simulations, which is described in the next section.

ADM method for geothermal systems

ADM solution strategy

The linear system (4) describes a fully-resolved fine-scale discrete equation. ADM method provides a solution to this system on a dynamic multilevel grid, in an algebraic procedure, the resolution of which is defined based on an error-estimate (front-tracking) based strategy. The fine-scale grid containing $N_f = N_{fx} \times N_{fy} \times N_{fz}$ grid cells is considered. ADM imposes set of n_l levels of hierarchically nested coarse grids, with coarsening ratio of $\gamma_x^l \times \gamma_y^l \times \gamma_z^l$. Here, the index l refers to the level of coarsening (i.e., $l = 0$ corresponds to fine-scale resolution and $l = n$ represents the n^{th} level of coarsening). Therefore,

$$\gamma^l = (\gamma_x^l, \gamma_y^l, \gamma_z^l) = (\frac{N_{fx}}{N_{lx}}, \frac{N_{fy}}{N_{ly}}, \frac{N_{fz}}{N_{lz}}) \tag{5}$$

holds. The ADM grid at each time-step (where solution is provided) is constructed as uniun of grid-cells at different resolutions in different part of the domain. The mapping of fine-scale system to the dynamic multilevel grid is achieved algebraically by applying sequences of restriction (**R**) and prolongation (**P**) operators. Therefore, at each iteration, the ADM system reads

$$\underbrace{\hat{\mathbf{R}}_l^{l-1} \dots \hat{\mathbf{R}}_1^0 \mathbf{J_0} \hat{\mathbf{P}}_0^1 \dots \hat{\mathbf{P}}_{l-1}^l}_{\mathbf{J}_{ADM}} \delta\hat{x}_l = -\underbrace{\hat{\mathbf{R}}_l^{l-1} \dots \hat{\mathbf{R}}_1^0 r_0}_{r_l}, \tag{6}$$

where $\hat{\mathbf{R}}_l^{l-1}$ is the restriction operator that maps the part of the vector of solutions which are at resolution $l-1$ ($\delta\hat{x}_{l-1}$) to resolution l ($\delta\hat{x}_l$). Correspondingly, $\hat{\mathbf{P}}_l^{l+1}$ is the prolongation operator that maps the part of the entire solution vector which are at level l to level $l-1$. Once the system is solved at ADM resolution, the approximated solution at fine-scale resolution $\delta x_0'$ (reference fine-scale solution is represented as δx_0) can be achieved by

$$\delta x_0 \approx \delta x_0' = \hat{\mathbf{P}}_0^1 \dots \hat{\mathbf{P}}_{l-1}^l \, \delta x_l. \tag{7}$$

The static multilevel prolongation operator $\mathbf{P}_{i-1}^i$ is constructed for the entire domain. However, only a fraction of the domain needs to go through this map at each time-step. This dynamically constructed map, which is presented as $\hat{\mathbf{P}}_{i-1}^i$ in Eq. (6), is the so-called ADM prolongation operator. The static multilevel prolongation operator has a block structure as

$$\mathbf{P}_{i-1}^i = \begin{pmatrix} (P_p)_{i-1}^i & 0 & 0 \\ 0 & (P_{T_f})_{i-1}^i & 0 \\ 0 & 0 & (P_{T_r})_{i-1}^i \end{pmatrix}_{N_{i-1} \times N_i}. \tag{8}$$

Likewise, the static multilevel restriction operator reads

$$\mathbf{R}_i^{i-1} = \begin{pmatrix} (R_P)_i^{i-1} & 0 & 0 \\ 0 & (R_{T_f})_i^{i-1} & 0 \\ 0 & 0 & (R_{T_r})_i^{i-1} \end{pmatrix}_{N_l \times N_{l-1}}. \tag{9}$$

Here, the multilevel restriction operator is finite-volume based as to ensure mass conservation on multilevel ADM grid.

In this work, $(P_p)_{i-1}^i$ and $(P_{T_r})_{i-1}^i$ blocks are constructed following a multilevel multiscale procedure For fluid temperature. However, the prolongation block for fluid temperature is defined as $(P_{T_f})_{i-1}^i = [(R_{T_f})_i^{i-1}]^T$, where the superscript T indicates the transpose operator.

Grid selection criterion

In this work, at each time step n, the grid resolution is chosen explicitly (based on the solution at time-step $n-1$) by employing a temperature based criterion. Let Ω_l^I and Ω_l^J be the set of two neighbouring coarser cells I and J at resolution level l, which contain the index of all finer resolution cells they include. Also, i and j are fine cell indices, belonging to the sets Ω_l^I and Ω_l^J, respectively. The criteria for grid refinement can be defined as

$$\Delta\bar{T}_{IJ} = \frac{max\big(|T_i - T_j|\big)}{|T_{\text{inj}} - T_{\text{prod}}|} \quad \forall\, i \in \Omega_l^I \;\text{ and }\; \forall\, j \in \Omega_l^J. \tag{10}$$

Here, T_{inj} and T_{prod} are the injection and production temperatures, respectively. A grid-block I at grid resolution level l is refined to resolution $(l-1)$ if

$$\Delta\bar{T}_{IN} > \text{tol}, \tag{11}$$

where, N indicates all grid-blocks at resolution l neighbouring cell I. For the numerical examples of this article, the variable used for the coarsening criterion is the fluid temperature. Additionally, refinement is imposed around wells to ensure that the effect of source terms is captured accurately.

Numerical results for two 2D test cases are presented, as a proof of concept, in the next section.

Numerical results

A 2D 216 m $\times$ 54 m geothermal reservoir is considered with both a homogeneous (case 1) and a heterogeneous (case 2) permeability fields. A 216×54 Cartesian grid is imposed on the domain. A cold water injector well is present in the bottom left corner of the reservoir whereas a production well is situated in the top right corner. Both wells are pressure-constrained with bottom hole pressures of 300MPa and 10MPa, for injection and production respectively. The temperature of injected water is at 300K whereas the reservoir has an initial temperature of 400K. No-flow boundary condition is considered for all boundaries. The fluid and rock properties employed are presented in Table 1. The correlations to compute the remaining fluid properties are available in the Appendix.

Table 1 *Fluid and rock properties.*

Property	value
Rock conductivity (D)	$4\,\frac{\text{J}}{\text{s m K}}$
Rock density (ρ_r)	$2750\,\frac{\text{kg}}{\text{m}^3}$
Rock specific heat (C_{p_r})	$790\,\frac{\text{J}}{\text{kg·K}}$
Porosity (ϕ)	0.2
Grain diameter	0.001 m
Fluid specific heat (C_{p_f})	$4200\,\frac{\text{J}}{\text{kg·K}}$
Fluid conductivity (k_f)	$0.591\,\frac{\text{J}}{\text{s m K}}$

The accuracy of the ADM method is studied by comparing its results against those obtained by fine-scale simulations. The performance of ADM is reported in fraction of number of active grid cells compared to total number of fine-scale grid cells. The ADM error at time step t is calculated as

$$\varepsilon_x(t) = \frac{\|x_{FS}(t) - x_{ADM}(t)\|_2}{\|x_{FS}(t)\|_2}, \tag{12}$$

where, x represents a generic variable (i.e., p or T) and the subscript FS refers to fine-scale. The sensitivity of ADM results to the tolerance employed for the coarsening criterion is also studied.

Test Case 1: 2D homogeneous reservoir

An isotropic homogeneous permeability, $K = 10^{-15}$ m^2, is considered. All simulations are run until 300 days of injection is reached.

Figure 1 shows a comparison between ADM with coarsening criterion of 5% as described in Eq. (11). It can be seen from Fig. 1 that the resolution is kept at fine-scale resolution around wells and on the area surrounding the temperature front. Note that the diffuse temperature front is well captured by the ADM method.

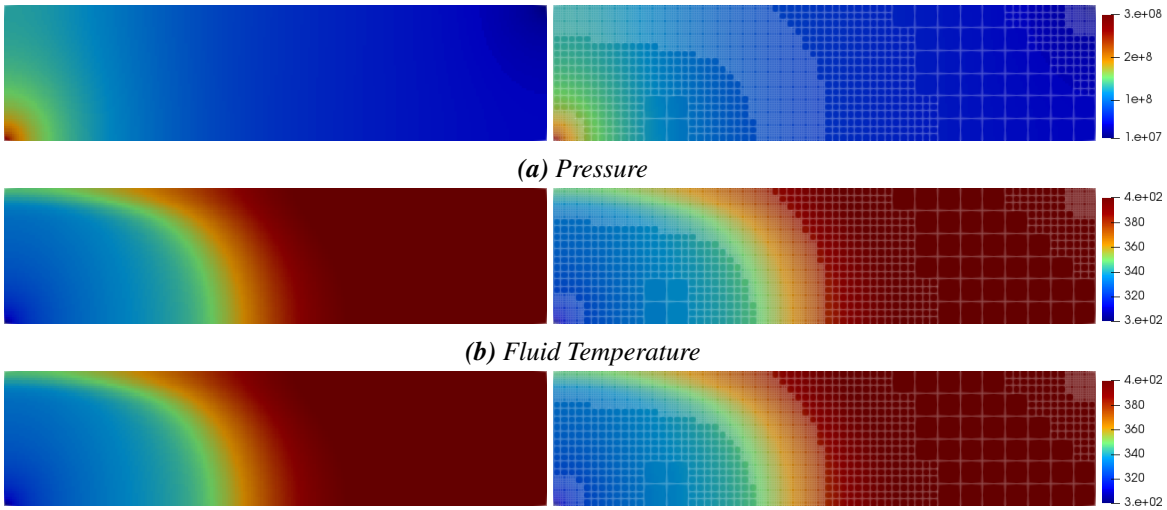

(a) *Pressure*

(b) *Fluid Temperature*

(c) *Rock Temperature*

Figure 1 *Pressure, fluid temperature, and rock temperature solution after* 300 *days of injection in homogeneous reservoir. Fine-scale solution (left) is approximated by ADM solution with* 5% *tolerance (right).*

Figure 2 shows ADM errors, as described in Eq. (12), for each time step. Smaller tolerance value (i.e., higher sensitivity to temperature changes) leads to higher percentages of active grid cells involved during simulation and consequently more accurate results. Note that at the beginning of the simulation, coarser grids are employed regardless of what tolerance value is employed and the region around the wells are always kept at fine-scale resolution.

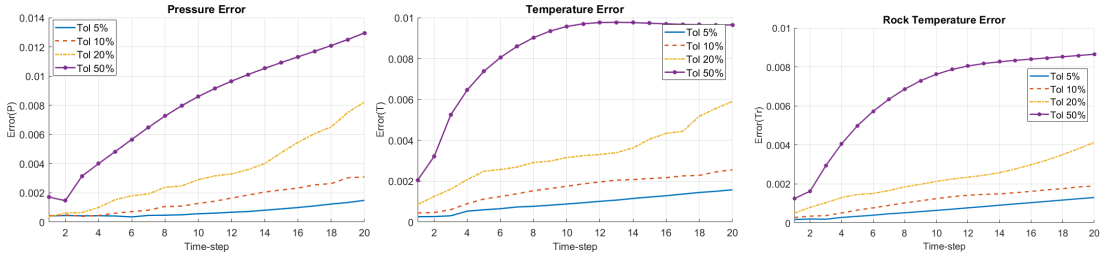

(a) *Pressure Error* ***(b)*** *Temperature Error* ***(c)*** *Rock Temperature Error*

Figure 2 *Error of ADM solution (pressure, fluid temperature and rock temperature) with* $5\%, 10\%, 20\%$ *and* 50% *tolerances compared to fine-scale solution in homogeneous reservoir.*

Figure 3 (left) shows the percentage of active grid cells employed over 20 simulation time-steps. In general, number of active grid cells increases as the temperature front progresses from injection well. Thereafter, by advancement of the temperature front, number of active grid cells increases to a plateau and may start decreasing again due to employment of more coarse grid cells are in the area with lower temperature changes. Moreover, Fig. 3 (right) shows the average errors and average fraction of the ADM active grid cells over the whole simulation time. It can be seen that the average error increases proportionally to ADM tolerance.

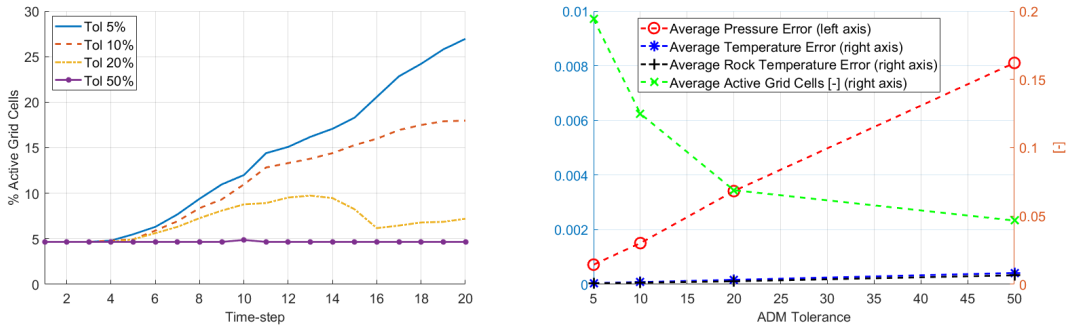

Figure 3 *Percentage of active grid cells for each time step for different tolerances (left), and average error and active grid cells with respect to ADM tolerance (right).*

Test Case 2: 2D heterogeneous reservoir

A 2D heterogeneous reservoir which is populated with isotropic permeability field extracted from SPE10 top layer is considered and shown in Fig. 4.

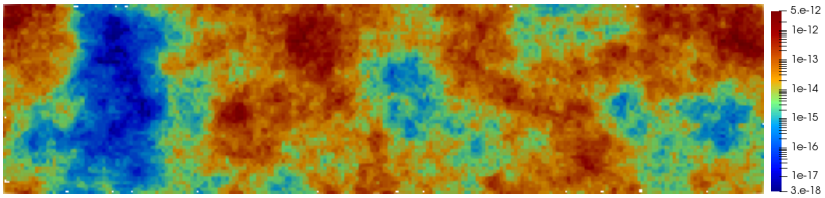

Figure 4 *The heterogeneous isotropic permeability field used in test case 2.*

Figure 5 presents the simulation results of pressure, fluid temperature and rock temperature. Similar to the results of test case 1, ADM is able to track the temperature front by keeping fine-scale grid resolution neighbouring the front, while applying coarser grids where fine-scale is not needed. In regions with higher permeability, temperature front advances further due to convection dominance. Consequently, one might observe non-unified distribution of fine-grid cells.

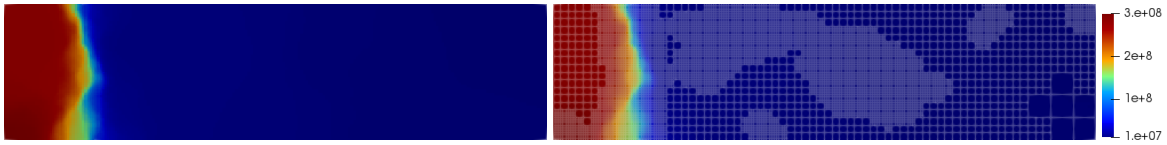

(a) *Pressure*

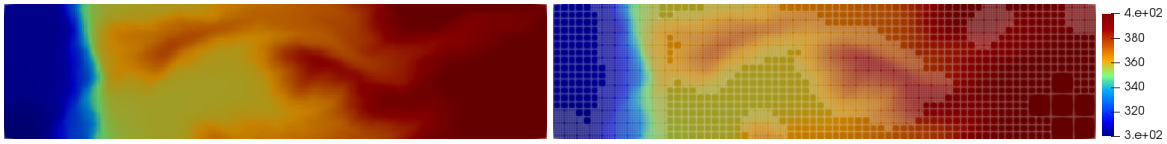

(b) *Fluid Temperature*

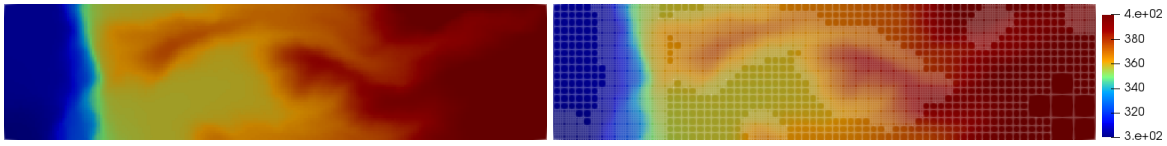

(c) *Rock Temperature*

Figure 5 *Pressure, fluid temperature, and rock temperature solution after* 300 *days of injection in heterogeneous reservoir. Fine-scale solution (left) is approximated by ADM solution with* 5% *tolerance (right).*

The error between ADM and fine-scale solution for each time step is presented in Fig. 6. It can be seen

that a good approximation of fine-scale solution is provided by ADM, by applying only a fraction of the fine-scale grid cells.

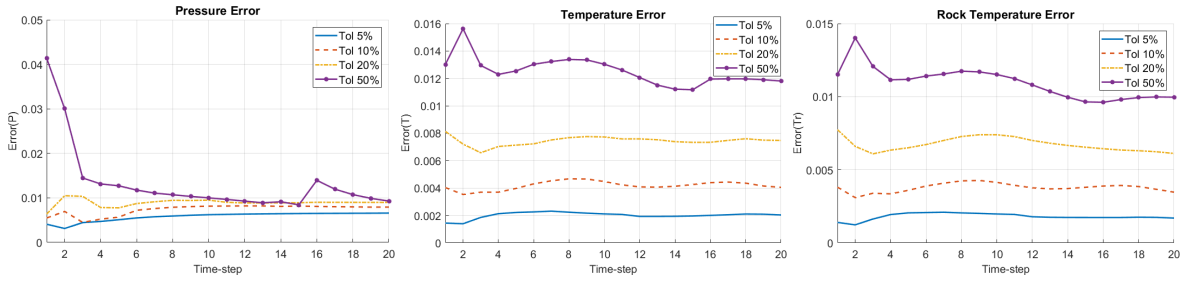

(a) Pressure Error *(b) Temperature Error* *(c) Rock Temperature Error*

Figure 6 *Error of ADM solution with 5% tolerance compared to fine scale solution in heterogeneous reservoir.*

Figure 7 (left) shows the percentage active grid cells versus simulation time-steps. Number of grids employed is dynamically changing based on evolution of temperature front in the reservoir. Figure 7 (right) shows average of errors and active grid cells over the entire simulation time, which involves 20 time steps.

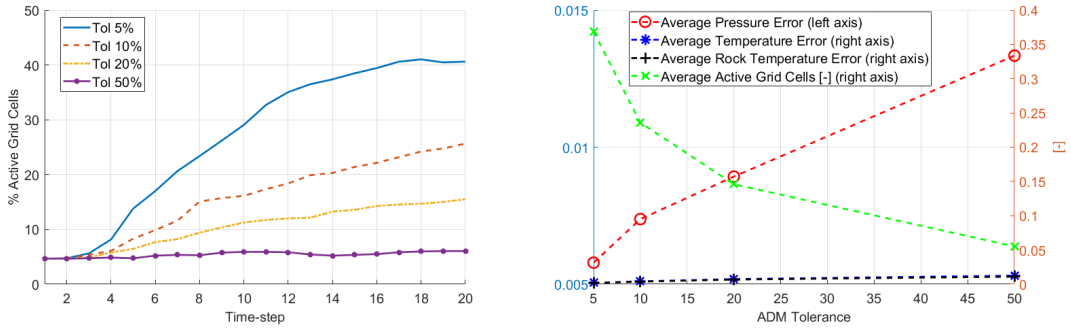

Figure 7 *Percentage of active grid cells versus simulation time-steps for different tolerances (left), and average error and active grid cells with respect to ADM tolerance (right). These plots are provided for heterogeneous test case.*

Conclusions

An Algebraic Dynamic Multilevel method for fully-coupled simulation of thermal single phase flow was presented in this work. Here, the fine-scale system is mapped in to a multilevel dynamic grid using a sequence of multilevel restriction and prolongation operators. The fine-scale resolution is used around the wells and on the position of the temperature front (detected via the coarsening criterion). However, different levels of coarse grids are employed wherever the fine-scale resolution is not needed.

Numerical results for 2D homogeneous and heterogeneous test cases were presented. ADM results on both test cases were compared to fine-scale solution. Moreover, The sensitivity of ADM to different tolerances of coarsening criterion on fluid temperature was studied. The results, with different amount of dynamic active grid cells, show that ADM is able to provide accurate results by employing only a fraction of the fine-scale grid cells in the domain. Note that despite allowing for non-thermal equilibrium between fluid and rock, for the studied cases, the fluid and rock temperatures were quite close. The rarefaction of the fluid temperature profile (highly diffused temperature front) results in the employment of more fine-scale grid cells in the region surrounding the cold front. Obviously, the convection-conduction ratio influences the sharpness of the temperature front. Nevertheless, the ADM provides a robust algebraic framework which provides a scalable simulation method for non-isothermal fluid flows.
One can assume that by increasing the size of the domain, the average percentage of active grid cells

reduces. Therefore, ADM casts a promising simulation approach for real-field geothermal reservoir simulations.

Acknowledgment

The authors thank Delft Advanced Reservoir Simulation (DARSim) group members for the fruitful discussions towards the successful development of the geothermal-ADM method.

References

Al-Shemmeri, T. [2012] *Engineering Fluid Mechanics*, chap. 1. Bookboon, 18.

Axelsson, G., Stefansson, V. and Xu, Y. [2003] Sustainable management of geothermal resources. In: *In Proceedings of the International Geothermal Conference*. 40–48.

Bertani, R. [2012] Geothermal power generation in the world 2005?2010 update report. *Geothermics*, **41**, 1–29.

Bosma, S., Hajibeygi, H., Tene, M. and Tchelepi, H.A. [2017] Multiscale finite volume method for discrete fracture modeling on unstructured grids (MS-DFM). *Journal of Computational Physics*, **351**, 145 – 164.

Burnell, J., Clearwater, E., A., C., Kissling, W., OSullivan, J., OSullivan, M. and Yeh, A. [2012] Future directions in geothermal modelling. In: *In Proceedings (electronic) 34rd New Zealand Geothermal Workshop*. 19–21.

Burnell, J., OSullivan, M., OSullivan, J., Kissling, W., Croucher, A., Pogacnik, J., Pearson, S., Caldwell, G., Ellis, S., Zarrouk, S. and Climo, M. [2015] Geothermal supermodels: the next generation of integrated geophysical, chemical and flow simulation modelling tools. In: *In Proceedings World Geothermal Congress*. 19–21.

Coats, K.H. [1977] Geothermal Reservoir Modelling. In: *SPE Annual Fall Technical Conference and Exhibition*.

Cusini, M., van Kruijsdijk, C. and Hajibeygi, H. [2016] Algebraic dynamic multilevel (ADM) method for fully implicit simulations of multiphase flow in porous media. *Journal of Computational Physics*, **314**, 60–79.

David, D. and Jenny, S. [2016] Collective properties of injection induced earthquake sequences: 1. Model description and directivity bias. *Journal of Geophysical Research: Solid Earth*, **121**(5), 3609–3637.

Deb, R. and Jenny, P. [2017] Finite volume-based modeling of flow-induced shear failure along fracture manifolds. *Int. J. for Numerical and Analytical Methods in Geomechanics*, **41**(18), 1922–1942.

Hajibeygi, H., Bonfigli, G., Hesse, M. and Jenny, P. [2008] Iterative multiscale finite-volume method. *J. Comput. Phys.*, **227**, 8604–8621.

Hou, T.Y. and Wu, X.H. [1997] A multiscale finite element method for elliptic problems in composite materials and porous media. *J. Comput. Phys.*, **134**, 169–189.

Jenny, P., Lee, S.H. and Tchelepi, H.A. [2003] Multi-scale finite-volume method for elliptic problems in subsurface flow simulation. *J. Comput. Phys.*, **187**, 47–67.

Leal, A.M.M., Kulik, D.A., Smith, W.R. and Saar, M.O. [2017] An overview of computational methods for chemical equilibrium and kinetic calculations for geochemical and reactive transport modeling. *Pure and Applied Chemistry*, **89**(5), 597 – 643.

Lund, J.W., Freeston, D.H. and Boyd, T.L. [2011] Direct utilization of geothermal energy 2010 worldwide review. *Geothermics*, **40**(3), 159–180.

Morel, F. and Morgan, J. [1972] Numerical method for computing equilibriums in aqueous chemical systems. *Environmental Science & Technology*, **6**(1), 58 – 67.

Møyner, O. and Lie, K.A. [2016] A multiscale restriction-smoothed basis method for high contrast porous media represented on unstructured grids. *Journal of Computational Physics*, **304**, 46–71.

Nield, D.A. and Bejan, A. [2006] *Convection in Porous Media*. Springer.

Norbeck, J.H. and Horne, R.N. [2016] Evidence for a transient hydromechanical and frictional faulting response during the 2011 Mw 5.6 Prague Oklahoma earthquake sequence. *Journal of Geophysical Research: Solid Earth*, **121**(12), 8688 – 8705.

Norbeck, J.H., McClure, M.W. and Horne, R.N. [2018] Field observations at the Fenton Hill enhanced

geothermal system test site support mixed-mechanism stimulation. *Geothermics*, **74**, 135–149.
OSullivan, M.J., Pruess, K. and Lippmann, M.J. [2001] State of the art of geothermal reservoir simulation. *Geothermics*, **30**(4), 395–429.
Parramore, E., Edwards, M.G., Pal, M. and Lamine, S. [2016] Multiscale Finite-Volume CVD-MPFA Formulations on Structured and Unstructured Grids. *SIAM Multiscale Model. Simul.*, **14**, 559 – 594.
Praditia, T., Helmig, R. and Hajibeygi, H. [2018] Multiscale formulation for couple. *Computat. Geo.*, **(in press)**, DOI: 10.1007/s10596–018–9754–4.
Rossi, E., Kant, M.A., Madonna, C., Saar, M.O. and von Rohr, P.R. [2018] The Effects of High Heating Rate and High Temperature on the Rock Strength: Feasibility Study of a Thermally Assisted Drilling Method. *Rock Mechanics and Rock Engineering*.
Wagner, W. and Kretzschmar, H. [2008] *International Steam Tables - Properties of Water and Steam based on the Industrial Formulation IAPWS-IF97*. Springer, second edn.
Wang, Y., Hajibeygi, H. and Tchelepi, H.A. [2014] Algebraic Multiscale Linear Solver for Heterogeneous Elliptic Problems. *J. Comput. Phys.*, **259**, 284–303.
Wong, Z.Y., Horne, R.N. and Tchelepi, H.A. [2018] Sequential implicit nonlinear solver for geothermal simulation. *Journal of Computational Physics*, **368**, 236 – 253.
Zeng, Z. and Grigg, R. [2006] A Criterion for Non-Darcy Flow in Porous Media. In: *Transport in Porous Media*, 63. 57–69.

Appendix: correlations

The following correlations were employed to compute fluid and rock properties in the numerical experiments.

Fluid viscosity: Viscosity-temperature relationship reads (Al-Shemmeri, 2012)

$$\mu_f(T) = 2.414 \times 10^{-5} \times 10^{\frac{247.8}{T-140}}.$$

Fluid density: Fluid density is defined as function of pressure and temperature (Coats, 1977) as

$$\rho_f(P,T) = \rho_{fs}(T)\left[1 + c_w(T)(P - P_s)\right],$$

where $P_S = 1\,\text{bar}$. $c_w(T)$ and $\rho_{fs}(T)$ are obtained from empirical correlations (Praditia et al., 2018; Wagner and Kretzschmar, 2008), i.e.,

$$c_w(T) = \left(0.0839T^2 + 652.73T - 203714\right) \times 10^{-12}$$

$$\rho_{fs}(T) = -0.0032T^2 + 1.7508T + 757.5.$$

Fluid Entalphy: Fluid entalphy is defined as function of pressure and temperature (Coats, 1977) as

$$H_f(P,T) = u_{ws} + C_{pf}(T - T_s) + \frac{P}{\rho_f},$$

where $u_{ws} = 420000\frac{\text{J}}{\text{kg}}$.

Heat exchange coefficient: Heat exchange coefficient h is given as (Nield and Bejan, 2006)

$$\frac{1}{h} = \frac{D_p}{N_u k_f} + \frac{D_p}{10\,D},$$

where D_p is the grain diameter and D is the rock heat conductive coefficient. Note that N_u is the Nusselt number, which is defined as

$$N_u = \frac{0.225}{\phi} P_r^{0.33} R_e^{0.67},$$

where P_r (Nield and Bejan, 2006) and R_e (Zeng and Grigg, 2006) are the Prandtle and Reynolds numbers, respectively, i.e.,

$$P_r = \frac{C_{pf}\mu_f}{k_f}.$$

and

$$R_e = \frac{\rho_f V D_p}{\mu_f}.$$

Here V is the Darcy velocity.